Analysis of groundwater flow and stream depletion in the L-shaped fluvial aquifer

Chao-Chih Lin[1], Ya-Chi Chang[2] and Hund-Der Yeh[1]

[1]Institute of Environmental Engineering, National Chiao Tung University, Hsinchu, Taiwan

5 [2]Taiwan Typhoon and Flood Research Institute, National Applied Research Laboratories, Taipei, Taiwan

Correspondence to: Hund-Der Yeh (hdyeh@mail.nctu.edu.tw)

Abstract. Understanding the head distribution in aquifers is crucial for the evaluation of groundwater resources. This article develops a model for describing flow induced by pumping in an L-shaped fluvial aquifer bounded by impermeable bedrocks and two nearly fully penetrating streams. A similar scenario for numerical studies was reported in Kihm et al. (2007). The

10 water level of the streams is assumed to be linearly varying with distance. The aquifer is divided into two sub-regions and the continuity conditions of hydraulic head and flux are imposed at the interface of the sub-regions. The steady-state solution describing the head distribution for the model without pumping is first developed by the method of separation of variables. The transient solution for the head distribution induced by pumping is then derived based on the steady-state solution as initial condition and the methods of finite Fourier transform and Laplace transform. Moreover, the solution for stream depletion rate

15 (*SDR*) from each of the two streams is also developed based on the head solution and Darcy's law. Both head and *SDR* solutions in real time domain are obtained by a numerical inversion scheme called the Stehfest algorithm. The software MODFLOW is chosen to compare with the proposed head solution for the L-shaped aquifer. The steady-state and transient head distributions within the L-shaped aquifer predicted by the present solution are compared with the numerical simulations and measurement data presented in Kihm et al. (2007). The *SDR* solution is employed to demonstrate its use as a design tool in determining well

20 location for required amounts of *SDR* from nearby streams under a specific aquifer pumping rate.

1 Introduction

Groundwater is an important water resource for agricultural, municipal and industrial uses. The planning and management of water resources through the investigation of the groundwater flow is one of the major tasks for practicing engineers. The aquifer type and shape are important factors influencing the groundwater flow. Many studies have been devoted to the

25 development of analytical models for describing flow in finite aquifers with a rectangular boundary (e.g., Chan et al., 1976; Chan et al., 1977; Daly and Morel-Seytoux, 1981; Latinopoulos, 1982; Corapcioglu et al., 1983; Latinopoulos, 1984, 1985; Lu et al., 2015), a wedge-shaped boundary (Chan et al., 1978; Falade, 1982; Holzbecher, 2005; Yeh et al., 2008; Chen et al., 2009; Samani and Zarei-Doudeji, 2012; Samani and Sedghi, 2015; Kacimov et al. 2016), a triangle boundary (Asadi-Aghbolaghi et al., 2010) a trapezoidal-shaped boundary (Mahdavi and Seyyedian, 2014), or a meniscus-shaped domain

(Kacimov et al. 2017). So far, the case of re-entrant angle (L-shaped) boundaries has been treated analytically in different fields such as torsion of elastic bars (Kantorovich and Krylov, 1958), head fluctuation problems for tidal aquifers (Sun, 1997; Li and Jiao, 2002), and heat conduction in plates (Mackowski, 2011). However, none of them are to deal with pumping or stream depletion problems.

5   Many studies focused on the development of numerical approaches for evaluating the groundwater flow in an aquifer with irregular domain and various types of boundary conditions. The rapid increase of the computing power of PC enables the numerical models to handle the groundwater flow problems with complicated geometric shapes and/or heterogeneous aquifer properties. We therefore adopt the software MODFLOW to assess the accuracy of the predictions by the present solution. Numerical methods such as finite element methods (FEMs) and finite difference methods (FDMs) are very commonly used in

10   engineering simulations or analyses. For the application of FEMs, Taigbenu (2003) solved the transient flow problems based on the Green element method for multi-aquifer systems with arbitrary geometries. Kihm et al. (2007) used a general multidimensional hydrogeomechanical Galerkin FEM to analyze three-dimensional (3D) problems of saturated-unsaturated flow and land displacement induced by pumping in a fluvial aquifer in Yongpoong 2 Agriculture District, Gyeonggi-Do, Korea. The domain of the aquifer is in L shape and bounded by streams and impermeable bedrock. They performed FEM simulations

15   for steady-state spatial distributions of hydraulic head before aquifer pumping and then for the distributions of hydraulic head and land displacement vector after one-year pumping. Their simulation results were compared and validated with the field measurements of hydraulic head and vertical displacement in the transient case.

The FDMs have been widely utilized in the groundwater problems too. Mohanty et al. (2013) evaluated the performances of the finite difference groundwater model MODFLOW and the computational model artificial neural network (ANN) in the

20   simulation of groundwater level in an alluvial aquifer system. They compared the results with field observed data and found that the numerical model is suitable for long-term predictions, whereas the ANN model is appropriate for short-term applications. Serrano (2013) illustrated the use of Adomian's decomposition method to solve a regional groundwater flow problem in an unconfined aquifer bounded by the main stream on one side, two tributaries on two sides, and an impervious boundary on the other side. He demonstrated an application to an aquifer bounded by four streams with a deep excavation

25   inside where the head was kept constant. Jafari et al. (2016) incorporated Terzaghi's theory of one-dimensional consolidation with MODFLOW to evaluate groundwater flow and land subsidence due to heavy pumping in a basin aquifer in Iran. So far, many computer codes developed based on either FDMs (e.g., FTWORK and MODFLOW), FEMs (e.g., AQUIFEM-N, BEMLAP, FEMWATER, and SUTRA) or boundary element methods (e.g., BEMLAP) had been employed to simulate a variety of groundwater flow problems (Loudyi et al., 2007).

30   On the other hand, analytical solutions are convenient and powerful tools to explore the physical insight of groundwater flow systems. The head solution is capable of predicting the spatiotemporal distribution of the drawdown at any location within the simulation time and the *SDR* solution can estimate the stream filtration rate at any instance at a specific location in the groundwater flow system. Thus, the development of analytical models for describing the groundwater flow in a heterogeneous aquifer with irregular outer boundaries and subject to various types of boundary condition is of practical use from an

engineering viewpoint. Kuo et al. (1994) applied the image well theory and Theis' equation to estimate transient drawdown in an aquifer with irregularly shaped boundaries. The aquifer is an oil reservoir bounded by three tortuous faults. However, the number of the image wells should be largely increased if the aquifer boundary is asymmetric and rather irregular. Insufficient number of the image wells might result in poor results or even divergence (Matthews et al., 1954). Read and Volker (1993)

5 presented analytical solutions for steady seepage through hillsides with arbitrary flow boundaries. They used the least squares method to estimate the coefficients in a series expansion of the Laplace equation. Li et al. (1996) extended the results of Read and Volker (1993) in solving the two-dimensional (2D) groundwater flow in porous media governed by Laplace's equation involving arbitrary boundary conditions. The solution procedure was obtained by means of an infinite series of orthonomal functions. Additionally, they also introduced a method, called image-recharge method, to establish the recurrence relationship

10 of the series coefficients. Patel and Serrano (2011) solved nonlinear boundary value problems of multidimensional equations by Adomian's method of decomposition for groundwater flow in irregularly shaped aquifer domains. Mahdavi and Seyyedian (2014) developed a semi-analytical solution for hydraulic head distribution in trapezoidal-shaped aquifers in response to diffusive recharge of constant rate. The aquifer was surrounded by four fully penetrating and constant-head streams. Kacimov et al. (2016) used the Strack-Chernyshov model to investigate the unconfined groundwater flows in a wedge-shaped

15 promontories with accretion along the water table and outflow from a groundwater mound into draining rays. Huang et al. (2016) presented 3D analytical solutions for hydraulic head distributions and *SDR*s induced by a radial collector well in a rectangular confined or unconfined aquifer bounded by two parallel streams and no-flow boundaries. Currently, the distribution of groundwater flow velocity in a circular meniscus aquifer was investigated analytically by theory of holomorphic functions and numerically by FEM (Kacimov et al., 2016).

20 Groundwater pumping near a stream in a fluvial aquifer may cause the dispute of stream water right, impact of aquatic ecosystem in stream, as well as water allocation or management problems for agriculture, industry, and municipality. The impacts of groundwater extraction by wells should therefore be thoroughly investigated before pumping. This paper develops a 2D mathematical model for describing the groundwater flow in an approximately L-shaped fluvial aquifer which is very close to the case of numerical simulations reported in Kihm et al. (2007). The aquifer is divided into two rectangular sub-

25 regions. The aquifer in each sub-region is homogeneous but anisotropic in the horizontal plane with principal direction aligned with the borderline of the rectangular sub-regions. Three types of boundary conditions including constant-head, linearly varying head, and no-flow are adopted to reflect the physical reality at the outer boundaries of the problem domain. A steady-state solution is first developed to represent the hydraulic head distribution within the aquifer before pumping. The transient head solution of the model is then obtained using the Fourier finite sine and cosine transforms and the Laplace transform. The

30 Stehfest algorithm is then taken to inverse Laplace-domain solution for the time-domain results. The software MODFLOW for the simulation of the 3D groundwater flow in L-shaped heterogeneous aquifer is used to evaluate the present head solutions. The *SDR* solution is also derived based on the head solution and Darcy's law and then used to evaluate the contribution of filtration water from each of two streams toward the pumping well.

2 Methodology

Figure 1 shows a fluvial plain located in Yongpoong 2 Agriculture District, Gyeonggi-Do, Korea reported in Kihm et al. (2007). The west side of the plain is a mountainous area with the formation of exposed impermeable bedrock and the east side has the Poonggye stream which passes the district from the southwest corner toward the northeast. A tributary of Poonggye stream, entering the stream with nearly a right angle, is on the north side of the plain. The Poonggye stream and its tributary are perennial streams and almost fully penetrate the fluvial aquifer system (Kihm et al., 2007). The width of Poonggye stream is about 15m reported in Rhms (2013).

2.1 Conceptual Model

The aquifer in the district is formed by fluvial deposit with a total thickness of 6 m, and consists of a clay loam aquitard of a thickness of about 2.5 m underlain by a loamy sand layer of a thickness of about 3.5 m (Kihm et al., 2007). In order to develop an analytical model for solving the groundwater flow, the domain of the aquifer in this study is approximated to be L-shaped, as delineated in Figure 2. Notice that in Figure 1 the solid line denotes the outer boundary of the L-shaped aquifer in this study while the dashed line represents the simulation area in the work of Kihm et al. (2007). The origin of the coordinate in Figure 2 is at the lower left corner of point A, which is at the intersection of boundary AB (i.e., a part of Poonggye stream) and boundary AG. The boundaries of the aquifer domain along EF and FG are impermeable bedrocks and thus regarded as impermeable boundaries. The annual average heads above the bottom of the aquifer are respectively identified as 5.18 m, 4.06 m and 5.29 m at points A, B, and D (Kihm et al., 2007). The hydraulic heads along AG and DE are assumed equal to their average head values as did in Kihm et al. (2007). In other words, the boundaries along AG and ED are assumed under the constant-head condition in our mathematical model. Physically, they are not streams and therefore not count for their contribution in the calculations of *SDR* in Sect. 2.5 Stream depletion rate. The boundaries AB and BD are designated to represent the Poonggye stream and its tributary, respectively. Kihm et al. (2007) fixed the hydraulic heads of Poonggye stream and its tributary at annual average water stages in their numerical simulations. Thus, this study considers that the stream has a perfect hydraulic connection with the aquifer and the stream stage varies linearly with distance. The average stream flow rate of the Poonggye stream with its tributary is about 100 m^3/s reported in Rhms (2013, p. 90). Pumping wells in the conceptual model are assumed to fully penetrate the aquifer near the perennial stream AB as mentioned in Kihm et al. (2007), and therefore the hydraulic gradient in vertical direction is neglected. Todd and Mays (2005, p. 232) noticed that the pumping rate in a shallow well with suction lift less than 7 m may range up to 500 m^3/day (0.01 m^3/s). Hence, the effect of pumping in a shallow well on the water table of nearby stream is generally negligible. The annual average depth from the ground surface to the water table is 1.26 m with a spatial variation from 0.57 m to 1.95 m in accordance with the average water stages in the streams AB and BD (Kihm et al., 2007). This depth was estimated under the hydrostatic equilibrium condition for the aquifer system before pumping and subject to the effect of net annual average rainfall. This aquifer is divided into two regions, named regions 1 and 2, and the hydraulic heads in these two regions are respectively expressed as $\phi_1(x, y, t)$ and $\phi_2(x, y, t)$.

2.2 Mathematical model

Consider that there are totally M pumping wells in region 1 and N pumping wells in region 2, and all the pumping wells fully penetrate the aquifer. The coordinates of kth well in region 1 is denoted as (x_{1k}, y_{1k}) and the associated pumping rate per unit thickness is Q_{1k} $[L^2/T]$. The governing equation describing the 2D hydraulic head distribution in region 1 is expressed as

$$K_{x1}\frac{\partial^2 \phi_1}{\partial x^2} + K_{y1}\frac{\partial^2 \phi_1}{\partial y^2} = S_{s1}\frac{\partial \phi_1}{\partial t} - \sum_{k=1}^{M} Q_{1k}\delta(x - x_{1k})\delta(y - y_{1k})$$

$$0 \leq x \leq l_1, 0 \leq y \leq d_1 \tag{1}$$

Similarly, the 2D hydraulic head distribution in region 2 for the l th well located at (x_{2l}, y_{2l}) with a pumping rate per unit thickness of Q_{2l} $[L^2/T]$ is

$$K_{x2}\frac{\partial^2 \phi_2}{\partial x^2} + K_{y2}\frac{\partial^2 \phi_2}{\partial y^2} = S_{s2}\frac{\partial \phi_2}{\partial t} - \sum_{l=1}^{N} Q_{2l}\delta(x - x_{2l})\delta(y - y_{2l})$$

$$l_2 \leq x \leq l_1, d_1 \leq y \leq d_2 \tag{2}$$

where S_s $[L^{-1}]$ represents the specific storage, $K_x[L/T]$ and $K_y[L/T]$ are the hydraulic conductivities in x- and y-direction, respectively. The symbol δ represents one dimensional (1D) Dirac's delta function $[1/T]$.

The boundary conditions for region 1 are expressed as:

$$\phi_1(0, y) = h_1 \text{ for AG} \tag{3}$$

$$\phi_1(l_1, y) = h_3 + \frac{h_2 - h_3}{b_2}y \text{ for BC} \tag{4}$$

$$\phi_1(x, 0) = h_1 + \frac{h_3 - h_1}{l_1}x \text{ for AB} \tag{5}$$

$$\frac{\partial \phi_1}{\partial y}(x, d_1) = 0 \text{ for GF} \tag{6}$$

Similarly, the boundary conditions for flow in region 2 are

$$\frac{\partial \phi_2}{\partial x}(l_2, y) = 0 \text{ for EF} \tag{7}$$

$$\phi_2(l_1, y) = h_3 + \frac{h_2 - h_3}{b_2}y \text{ for CD} \tag{8}$$

$$\phi_2(x, d_2) = h_2 \text{ for DE} \tag{9}$$

The continuity requirements of hydraulic head and flux along the interface CF are respectively

$$\phi_1(x, d_1) = \phi_2(x, d_1) \tag{10}$$

and

$$K_{y1} \frac{\partial \phi_1}{\partial y}\bigg|_{y=d_1} = K_{y2} \frac{\partial \phi_2}{\partial y}\bigg|_{y=d_1} \tag{11}$$

In order to express the solution in dimensionless form, the following dimensionless variables or parameters are introduced:

$\phi_1^* = (\phi_1 - h_1)/h_1$, $\phi_2^* = (\phi_2 - h_1)/h_2$, $t^* = K_{y1}t/S_{s1}d_2^2$, $\kappa_1 = K_{x1}/K_{y1}$, $\kappa_2 = K_{x2}/K_{y2}$, $x^* = x/l_1$, $y^* = y/d_2$, $d_1^* = d_1/d_2$, $l_2^* = l_2/l_1$, $Q_{1k}^* = d_2^2 Q_{1k}/K_{y1}h_1$ and $Q_{2l}^* = d_2^2 Q_{2l}/K_{y2}h_2$ where ϕ_1^* and ϕ_2^* stand for the dimensionless hydraulic heads in regions 1 and 2, respectively; t^* refers to the dimensionless time during the test; κ_1 and κ_2 represent the anisotropic ratio of hydraulic conductivity in region 1 and 2, respectively; x^* and y^* denote the dimensionless coordinates.

2.3 Steady-state solution for hydraulic head distribution

In order to compare the steady-state simulations of Kihm et al. (2007) without pumping, the steady-state solution for the hydraulic head distribution in the L-shaped aquifer is developed. Detailed derivation for the analytical solutions in steady state for regions 1 and 2 is given in Appendix A, and the results are expressed respectively as (Chu et al., 2012)

$$\phi_1^*(x^*, y^*) = \sum_{m=1}^{\infty} \Delta_1 [C_{1m}E_1(m, y^*) + F_1(m, y^*)] \sin(\lambda_m x^*) \tag{12}$$

and

$$\phi_2^*(x^*, y^*) = \sum_{n=1}^{\infty} \Delta_2 [D_{2n}E_2(n, y^*) + F_2(n, y^*)] \cos[\alpha_n(x^* - l_2^*)] \tag{13}$$

with

$$E_1(m, y^*) = \frac{e^{\Omega_{1m}y^*} - e^{-\Omega_{1m}y^*}}{e^{\Omega_{1m}b_1^*} - e^{-\Omega_{1m}b_1^*}} \tag{14}$$

$$F_1(m, y^*) = \frac{1}{\lambda_m}(-1)^{m+1}(h_{31}^* + h_{23}^* y^*) \tag{15}$$

$$E_2(n, y^*) = e^{-\Omega_{2n}y^*} - e^{\Omega_{2n}(y^*-2)} \tag{16}$$

$$F_2(n, y^*) = \frac{(-1)^{n-1}}{\alpha_n}(H_{31}^* + H_{23}^* y^*) \tag{17}$$

where the symbols and dimensionless variables Δ_1, Δ_2, λ_m, α_n, Ω_{1m}, Ω_{2n}, h_{31}^*, h_{23}^*, H_{23}^* and H_{31}^* are defined in Table 1. The coefficients C_{1m} and D_{2n} can be determined simultaneously by the continuity conditions of hydraulic head and flux along the interface CF. The results are denoted as follows:

$$C_{1m} = \frac{\Delta_2}{2}\frac{K_{y2}}{K_{y1}}\frac{h_2}{h_1}\sum_{n=1}^{\infty}\left[D_{2n}\frac{E_2'(n,y^*)}{E_1'(m,y^*)}\bigg|_{y^*=b_1^*} + \frac{F_2'(n,y^*)}{E_1'(m,y^*)}\bigg|_{y^*=b_1^*}\right]G_1(m,n) - \frac{F_1'(m,y^*)}{E_1'(m,y^*)}\bigg|_{y^*=b_1^*} \tag{18}$$

and

$$D_{2n} = \frac{1}{\Delta_2}\frac{h_1}{h_2}\sum_{m=0}^{\infty}\left[C_{1m}\frac{E_1(m,d_1^*)}{E_2(n,d_1^*)} + \frac{F_1(m,d_1^*)}{E_2(n,d_1^*)}\right]G_2(m,n) - \frac{F_2(n,d_1^*)}{E_2(n,d_1^*)} \tag{19}$$

with

$$E_1'(m, y^*) = \frac{\partial E_1(m, y^*)}{\partial y^*}$$ (20)

$$E_2'(n, y^*) = \frac{\partial E_2(n, y^*)}{\partial y^*}$$ (21)

$$F_1'(m, y^*) = \frac{\partial F_1(m, y^*)}{\partial y^*}$$ (22)

5    $$F_2'(n, y^*) = \frac{\partial F_2(n, y^*)}{\partial y^*}$$ (23)

$$G_1(m, n) = \frac{\int_{l_2^*}^1 sin(\lambda_m x^*) cos[\alpha_n(x^* - l_2^*)]dx}{\int_0^1 sin^2(\lambda_m x^*)dx}$$ (24)

$$G_2(m, n) = \frac{\int_{l_2^*}^1 sin(\lambda_m x^*) cos[\alpha_n(x^* - l_2^*)]dx}{\int_{l_2^*}^1 cos^2[\alpha_n(x^* - l_2^*)]dx}$$ (25)

2.4 Transient solution for hydraulic head distribution

The semi-analytical solution of the model for transient hydraulic head distribution with the previous steady-state solution as
10   the initial condition is developed via the methods of finite sine transform, finite cosine transform and Laplace transform. The
detailed derivation for transient solution is given in Appendix B and the results of the dimensionless hydraulic heads in Laplace
domain for regions 1 and 2 are respectively

$$\tilde{\phi}_1^*(x^*, y^*, p) = \delta_1 \sum_{i=1}^\infty [w_{1i}^* TE_1(i, y^*, p) + T_1(i, y^*, p) + T_2(i, y^*, p) + SQ_1(i, y^*, p)] sin(\lambda_i x^*)$$ (26)

and

15   $$\tilde{\phi}_2^*(x^*, y^*, p) = \delta_2 \sum_{j=1}^\infty [w_{2j}^* TE_2(j, y^*, p) + T_4(j, y^*, p) + T_5(j, y^*, p) + SQ_2(j, y^*, p)] cos[\alpha_j(x^* - l_2^*)]$$ (27)

with

$$TE_1(i, y^*, p) = \frac{e^{\mu_i(y^* - d_1^*)} - e^{-\mu_i(y^* + d_1^*)}}{1 - e^{-2\mu_i d_1^*}}$$ (28)

$$T_1(i, y^*, p) = \frac{1}{\mu_i p} [\theta_1^2 \lambda_i (-1)^i] [h_{31}^* e^{-\mu_i y^*} + (h_{23}^* y^* - h_{31}^*)] - h_{31}^* \frac{(-1)^i}{\lambda_i} e^{-\mu_i y^*}$$ (29)

$$T_2(i, y^*, p) = -C_{1m} \left[\frac{1}{2} - \frac{sin(2\lambda_i)}{4\lambda_i}\right] \left[\frac{-e^{-\Omega_{1i}(y^* - d_1^*)} + e^{\Omega_{1i}(y^* - d_1^*)}}{(1 - e^{2\Omega_{1i} d_1^*})(\Omega_{1i}^2 - \mu_i^2)} + \frac{\delta_1(-1)^i}{\mu_i^2}(h_{23}^* y^* + h_{31}^* - h_{31}^* e^{-\mu_i y^*})\right]$$ (30)

$$SQ_1(i,y^*,p) = \begin{cases} \frac{1}{2\mu_i p}\sum_{k=1}^{M} Q_{1k}^* \sin(\lambda_i x_{1k}^*) \frac{1}{1-e^{-\mu_i d_1^*}} \begin{bmatrix} e^{\mu_i(y_{1k}^*-2d_1^*)} + e^{\mu_i(y^*-y_{1k}^*-d_1^*)} \\ +e^{\mu_i(y_{1k}^*-y^*)} - e^{\mu_i(y^*-y_{1k}^*-2d_1^*)} \\ -e^{\mu_i(y_{1k}^*-y^*-d_1^*)} - e^{-\mu_i y_{1k}^*} \end{bmatrix}, y^* > y_{1k}^* \\[20pt] \frac{1}{2\mu_i p}\sum_{k=1}^{M} Q_{1k}^* \sin(\lambda_i x_{1k}^*) \frac{1}{1-e^{-\mu_i d_1^*}} \begin{bmatrix} e^{\mu_i(y^*-y_{1k}^*)} + e^{\mu_i(y_{1k}^*-2d_1^*)} \\ -e^{\mu_i(y^*+y_{1k}^*-2d_1^*)} - e^{-\mu_i y_{1k}^*} \end{bmatrix}, y^* < y_{1k}^* \end{cases} \tag{31}$$

$$TE_2(j,y^*,p) = \frac{e^{-\theta_j y^*} - e^{\theta_j(y^*-2)}}{e^{-\theta_j d_1^*} - e^{\theta_j(d_1^*-2)}} \tag{32}$$

$$T_4(j,y^*,p) = \left[\frac{\theta_2^2 \alpha_j (-1)^j}{p} + \frac{S_{s2} K_{y1}(-1)^j}{S_{s1} K_{y2} \alpha_j}\right] \left[\frac{H_{31}^* + H_{23}^* y^* - H_{21}^* e^{\theta_j(y^*-1)}}{\theta_j^2}\right] + \frac{H_{21}^*}{\alpha_j}\frac{(-1)^j}{p} e^{\theta_j(y^*-1)} \tag{33}$$

$$T_5(j,y^*,p) = -D_{2n}\frac{S_{s2} K_{y1}(1-l_2^*)}{2S_{s1} K_{y2}}\left(\frac{e^{\Omega_{2j}(y^*-2)} - e^{-\Omega_{2j}y^*}}{\theta_j^2 - \Omega_{2j}}\right) \tag{34}$$

$$SQ_2(j,y^*,p) = \begin{cases} \frac{1}{2\theta_j p}\sum_{l=1}^{N} Q_{2l}^* \cos(\alpha_j x_{2l}^*)\left(e^{-\theta_j(y^*-y_{2l}^*)} - e^{-\theta_j(2-y^*-y_{2l}^*)}\right), y^* > y_{2j}^* \\[14pt] \frac{1}{2\theta_j p}\sum_{l=1}^{N} Q_{2l}^* \cos(\alpha_j x_{2l}^*)\left(e^{\theta_j(y^*-y_{2l}^*)} - e^{-\theta_j(2-y^*-y_{2l}^*)}\right), y^* < y_{2j}^* \end{cases} \tag{35}$$

where p is the Laplace variable and the symbols or dimensionless parameters $\delta_1, \delta_2, \alpha_j, \lambda_i, \mu_i, \theta_1, \theta_2, \theta_j, \Omega_{1i}, \Omega_{2j}$ and H_{21}^* are introduced in Table 1.

The coefficients in Eqs. (26) and (27) are obtained via continuity requirements for the hydraulic head and flow flux at the interface CF. They can be solved simultaneously based on the following two equations

$$w_{1i}^* = \frac{K_{y2}}{K_{y1}}\frac{h_2}{h_1} G_1(i,j)\sum_{i=1}^{\infty}\left.\frac{w_{2j}^* TE_2'(j,y^*,p) + T_4'(j,y^*,p) + T_5'(j,y^*,p) + SQ_2'(j,y^*,p)}{TE_1'(j,y^*,p)}\right|_{y^*=d_1^*} + \sum_{i=1}^{\infty}\left.\frac{-T_1'(j,y^*,p) + T_2'(j,y^*,p) + SQ_1'(j,y^*,p)}{TE_1'(j,y^*,p)}\right|_{y^*=d_1^*} \tag{36}$$

and

$$w_{2j}^* = \frac{h_1}{h_2} G_2(j,i)\sum_{j=1}^{\infty}\left.\frac{w_{1i}^* TE_1(i,y^*,p) + T_1(i,y^*,p) - T_2(i,y^*,p) + SQ_1(i,y^*,p)}{TE_2(j,y^*,p)}\right|_{y^*=d_1^*} - \sum_{j=1}^{\infty}\left.\frac{T_4(j,y^*,p) + T_5(j,y^*,p) + SQ_2(j,y^*,p)}{TE_2(j,y^*,p)}\right|_{y^*=d_1^*} \tag{37}$$

with

$$TE_1'(i,y^*,p) = \frac{\partial TE_1(i,y^*,p)}{\partial y^*} \tag{38}$$

$$TE_2'(j,y^*,p) = \frac{\partial TE_2(j,y^*,p)}{\partial y^*} \tag{39}$$

$$T_1'(i,y^*,p) = \frac{\partial T_1(i,y^*,p)}{\partial y^*} \tag{40}$$

$$T_2'(i,y^*,p) = \frac{\partial T_2(i,y^*,p)}{\partial y^*} \tag{41}$$

$$T_4'(j,y^*,p) = \frac{\partial T_4(j,y^*,p)}{\partial y^*} \tag{42}$$

$$T_5'(j, y^*, p) = \frac{\partial T_5(j, y^*, p)}{\partial y^*} \tag{43}$$

$$SQ_1'(i, y^*, p) = \frac{\partial SQ_1(i, y^*, p)}{\partial y^*} \tag{44}$$

$$SQ_2'(j, y^*, p) = \frac{\partial SQ_2(j, y^*, p)}{\partial y^*} \tag{45}$$

The coefficient w_{2j}^* can be determined by substituting Eq. (36) into Eq. (37), the w_{1i}^* can then be obtained once w_{2j}^* is known. The hydraulic head distributions in real time domain can be obtained by applying a numerical Laplace inversion scheme, called the Stehfest algorithm (Stehfest, 1970), to Eqs. (26) and (27).

2.5 Stream depletion rate

Pumping in an aquifer near a stream will produce filtration water from the stream toward the well (Yeh et al., 2008). Water extracted from the pumping well comes from different sources such as nearby streams, constant-head boundaries, and aquifer storage. Since the boundaries AG and ED are not real stream in physical world and are mathematically treated as constant-head in models due to the fact that they are far from the pumping well, only the extraction rate from streams AB and BD near the pumping well needs to be considered. The extraction rate from the stream is referred to as stream depletion rate (*SDR*) and the dimensionless solutions of *SDR* in Laplace domain from the stream reaches AB and BD, denoted respectively as $\widetilde{SDR}_A$ and $\widetilde{SDR}_B$, can be estimated by taking the derivatives of Eqs. (26) and (27) with respect to y and x, respectively, then integrating along the reaches as:

$$\widetilde{SDR}_A = \frac{q_A}{Q} = -\frac{1}{Q} \int_0^{l_1} K_{y1} \left. \frac{\partial \widetilde{\phi}_1(x, y, p)}{\partial y} \right|_{y=0} dx \tag{46}$$

and

$$\widetilde{SDR}_B = \frac{q_B}{Q} = \frac{1}{Q} \left(\int_0^{d_1} K_{x1} \left. \frac{\partial \widetilde{\phi}_1(x, y, p)}{\partial x} \right|_{x=l_1} dy + \int_{d_1}^{d_2} K_{x2} \left. \frac{\partial \widetilde{\phi}_2(x, y, p)}{\partial x} \right|_{x=l_1} dy \right) \tag{47}$$

The total dimensionless stream depletion rate comes from the streams (AB and BD) is expressed as

$$SDR_T = SDR_A + SDR_B \tag{48}$$

Since the depletion rate from constant-head boundaries AG and DE which are far from the pumping well and can be neglected, the dimensionless SRR representing the storage release rate due to compression of aquifer matrix and expansion of groundwater in the pore space can be approximated as

$$SRR = 1 - SDR_T \tag{49}$$

3 Comparisons of present solution, numerical solutions and field observed data

3.1 Comparisons of present solution with MODFLOW solution

The software MODFLOW is used to simulate the groundwater flow due to pumping in the L-shaped aquifer in Yongpoong 2 Agriculture District with different hydraulic conductivities for the two layers. The MODFLOW is a widely used finite-difference model developed by U.S. Geological Survey for the simulation of 3D groundwater flow problems under various hydrogeological conditions (USGS, 2005). As shown in Figure 1, region 1 has an area of 852 m × 222 m (i.e., $l_1 \times d_1$) while the area of region 2 is 297 m × 183 m (i.e., $(l_1 - l_2) \times (d_2 - d_1)$). Thus, the total area of these two regions is 243495 m² which is close to the area of the fluvial aquifer (246500 m²) reported in Kihm et al. (2007). In the simulation of MODFLOW, the plane of the L-shaped aquifer is discretized with a uniform cell size of 3 m × 3 m. The aquifer thickness is 6 m and divided into two layers. The upper loam layer is 2.5 m and lower sand layer 3.5 m (Kihm et al. 2007). Within the aquifer domain, there is totally 54110 cells while the numbers of cell are 42032 and 12078 respectively for region 1 and region 2. The types of outer boundary specified for the L-shaped aquifer are the same as those defined in the mathematical model. The hydraulic heads along AG and DE are respectively $h_1 = 5.18$ m and $h_2 = 5.29$ m and the head at point B is $h_3 = 4.06$ m. The fluvial aquifer reported in Kihm et al. (2007) is isotropic and homogeneous in horizontal direction. In other words, the hydraulic conductivities in x and y directions are identical in both regions 1 and 2 (i.e., $K_{x1} = K_{y1} = K_{x2} = K_{y2} = K$). However, the aquifer is heterogeneous in the vertical direction. It has two layers with hydraulic conductivity $K_1 = 3 \times 10^{-6}$ m/s for the upper layer and $K_2 = 2 \times 10^{-4}$ m/s for the lower layer. The specific storage of the aquifer in both regions 1 and 2 is 10^{-4} m^{-1} (Kihm et al. 2007). Consider that the pumping well P_w is located at $(609 \text{ m}, 9 \text{ m})$ in region 1 shown in Figure 2 with a rate of 120 m³/day for one year pumping. The hydraulic head distribution predicted from the MODFLOW simulations is denoted as the dotted line shown in Figure 3.

A multi-layered aquifer with heterogeneous hydraulic conductivity may be approximated as an equivalent homogeneous medium. The equivalent hydraulic conductivity K_h may be evaluated as (Charbeneau, 2000):

$$K_h = \sum_i^m b_i K_i / \sum_i^m b_i \tag{50}$$

where K_i is the hydraulic conductivity in the horizontal direction for layer i, b_i is the thickness of layer i, and m is the number of the layers. Accordingly, the equivalent horizontal hydraulic conductivity K_h for the two layered L-shaped aquifer is estimated as 1.2×10^{-4} m/s. The hydraulic head distribution predicted by the present solution of Eqs. (26) and (27) and represented by the dotted line is shown in Figure 3. The figure indicates that the head distribution simulated by the present solution agrees with that by MODFLOW except the region near the no-flow boundary FG which has the largest relative deviation 2.1% between these two models. The comparison of the head distributions predicted by the present solution and MODFLOW ensures that the simplification of aquifer layers in the present model is appropriate and gives a fairly good predicted results.

3.2 Steady-state head distribution without pumping in Yongpoong 2 Agriculture District and impact of aquifer anisotropy

Kihm et al. (2007) reported the steady-state hydraulic head distribution, shown in Figure 4 by the dashed line, for the FEM simulation without groundwater pumping in the two-layered irregular aquifer. Figure 4 also shows the steady-state head distribution, denoted as the solid line, predicted by the present solution of Eqs. (11) and (12) for the L-shaped aquifer with $K_{x1} = K_{y1} = K_{x2} = K_{y2} = 1.2 \times 10^{-4}$ m/s (i.e., $\kappa_1 = \kappa_2 = 1$) evaluated based on Eq. (52) and other aquifer properties mentioned in Sect. 3.1. The contour lines of the head distribution are nearly parallel to the boundary AG and perpendicular to the boundary FG in the region $x \leq 200$ m. Moreover, the predicted heads within the regions between 500 m $\leq x \leq 852$ m and 0 m $\leq y \leq 200$ m are reasonably close to the FEM results, which range from 4.3 m to 4.7 m as shown in Figure 4. The groundwater flows toward point B since it has the lowest water table within the problem domain.

Figure 5 shows the contour lines of the hydraulic head distribution for isotropic case of $\kappa_1 = \kappa_2 = 1$ by the solid line and for anisotropic cases of $\kappa_1 = \kappa_2 = 4$ represented by the dashed dot line and $\kappa_1 = \kappa_2 = 0.25$ by the dashed line. In these three cases, the head distributions are significantly different in the region where $x \leq 600$ m for the head ranging from 5 m to 4.6 m. The largest head difference occurs near the upper boundary FG, reflecting the effects of no-flow condition and aquifer anisotropy on the flow pattern within this area.

3.3 Spatial head distributions due to pumping simulated by Kihm et al. (2007) and present solution after one year pumping

Note that Figure 3 shows the spatial head distributions in the L-shaped aquifer predicted by the present solution and the MODFLOW for one-year pumping at well P_w located at $(609$ m, 9 m$)$ with a rate of 120 m^3/day. In fact, Kihm et al. (2007) reported their FEM simulations for head distributions, groundwater flow velocity, and land displacement for one-year pumping at the well P_w with the same pumping rate mentioned above. They referred the simulated head results as initial steady-state distributions for the case of no pumping and final steady-state distributions for the case after one-year pumping. The aquifer configuration in their FEM simulations and the simulated head distributions denoted as dashed line are also demonstrated in Figure 3. The figure indicates that the present solution gives good predicted head contours near the pumping well and reasonably good result for the head distribution in region 1 as compared to those given by Kihm et al. (2007). The head distributions predicted by the FEM solution and present solution have obvious differences in the area far away from the pumping well. Those differences may be mainly caused by the difference in the physical domain considered in FEM solution and the simplified domain made in the present solution. In addition, the mathematical model in Kihm et al. (2007) considered the unsaturated flow and deformation of the unsaturated soil, which may also affect the head distribution after pumping. Notice that the pumping well is very close to the stream boundary AB, which is the main stream in that area and provides a large amount of filtration water to the well. Hence, it seems that the groundwater flows in the region 1 for $x \leq 300$ m (near boundary AG) and in the region 2 for $y \geq 200$ m (near boundaries FE and ED) are both far away from the well and almost not influenced by the pumping.

Three piezometers O_1, O_2 and O_3 were respectively installed at $(597\,\text{m}, 25\,\text{m})$, $(594\,\text{m}, 48\,\text{m})$ and $(597\,\text{m}, 204\,\text{m})$ mentioned in Kihm et al. (2007) and indicated in Figure 2. Note that O_1 was installed near the stream AB while O_3 was far away from the stream but close to the impermeable upper boundary. Figure 6 shows the temporal distributions of hydraulic head measured at these three piezometers (i.e., H_{iO}, $i = 1, 2, 3$) and predicted by the FEM simulations (Kihm et al., 2007) (i.e.,

5 H_{iF}), present solution (i.e., H_{iA}) and MODFLOW (i.e., H_{iM}). This figure indicates that the hydraulic heads predicted by the present solution has a good agreement with those simulated by Kihm et al. (2007). Compared with the field observation, the differences of predicted hydraulic head among FEM, present solution and MODFLOW are all less than 0.08 m at these three piezometers during 0.1 to 10 day. In addition, the largest relative differences between measured heads and predicted heads by the present solution at O_1 to O_3 during 0.1 to 5 day are respectively 1.64%, 1.74% and 0.62%, indicating that the present

10 solution gives good predictions in the early pumping period. Moreover, the effects of unsaturated flow and land deformation on the groundwater flow in Yongpoong aquifer are small and may be neglected. The hydraulic head at O_1 declines greater than those at O_2 and O_3 whereas the former is located closer to the pumping well P_w. Because P_w is very near the stream, the extracted water will be quickly contributed from the stream and therefore the drawdown at O_1 will be soon stabilized. Figure 6 indicates that the hydraulic heads at O_1 - O_3 predicted by the present solution reach steady state after $t = 100$ days, 220 days

15 and 290 days, respectively.

3.4 Stream filtration in fluvial aquifer systems

Stream filtration can be considered as a problem associated with the interaction between the groundwater and surface water. The pumped water originated from the nearby stream is commonly supplied for irrigation, municipalities, and rural homes. In stream basins with several tributaries, pumping wells are often installed adjacent to the confluence of two tributaries in fluvial

20 aquifers (Lambs, 2004).

It is of practical interest to know the temporal *SDR* distributions from both streams in the Yongpoong area when subject to pumping at P_w under a rate of 120 m³/day. The distances from P_w to the streams AB and BD are respectively 9 m and 243 m. Figure 7 shows the temporal *SDR* distribution from each stream, indicating that *SDR_A* (i.e., *SDR* from stream AB) is significantly larger than *SDR_B* (*SDR* from stream BD) all the time. The steady-state values for *SDR_A* and *SDR_B* are respectively

25 0.81 and 0.19 when $t \geq 220$ day. This is due to the fact that pumping well is closer to stream AB than stream BD and therefore water contributing to the pumping well from stream AB is much more than from stream BD. Figure 7 also shows that the *SDR_T* is zero and the aquifer storage release rate *SRR* is unity when $t \leq 0.01$ day, indicating that the well discharges totally from the aquifer storage at early time. Once the drawdown cone reaches the stream, the *SDR_T* increases quickly with time while the *SRR* decreases continuously over the entire pumping period. It is interesting to mention that S*DR_T* starts to contribute more water

30 to the pumping than *SRR* when $t \geq 5$ day. Finally, the S*DR_T* reaches unity and the *SRR* equals zero after $t \geq 220$ days, indicating that the aquifer system approaches steady state and all the extraction water comes from the streams.

3.5 Determination of well location for a specific *SDR* in a L-Shaped aquifer

It is of interest to mention that the present solution can be a preliminary design tool in determining the location of a pumping well in an L-shaped aquifer if the amounts of *SDR_A* and *SDR_B* had been determined by water authority or based on water right. Driscoll (1986, p. 615) mentioned that a well shall be installed at least 45.7 m from areas of spray materials, fertilizers or chemicals that contaminate the soil or groundwater. Hence, the distance from the pumping well to the stream is considered at least 50 m to guarantee the quality of extracted water.

Two specific values of *SDR_A*, 0.65 and 0.75, are considered for a water supply rate of 120 m^3/day. The present solution is employed to determine the well locations in order to meet the water need for irrigation in an L-shaped aquifer. Since stream AB is the main stream, it is better to extract more filtration water from it than from its tributary, stream BD. Therefore, four trial pumping wells, P_1 to P_4, are considered to install for the distances d_{B1} to d_{B4} of 50 m, 100 m, 150 m and 200 m, respectively, with $d_A = 50$ m indicated in Figure 2. The steady-state *SDR_A* predicted by the present solution for pumping at each of P_1 to P_4 with an extraction rate of 120 m^3/day is respectively 0.52, 0.61, 0.74, and 0.78. The least-squares equation with second degree polynomial for d_B in terms of *SDR_A* is $d_B = 591.4x^2 - 239.9x + 18.01$ with x representing the *SDR_A*. The estimated d_B for $SDR_A = 0.65$ and 0.75 by the regression equation are 111.95 m and 170.76 m, respectively. The predicted *SDR_A* from the present solution is 0.63 and its relative difference is 3.0% for pumping well located at (111.95 m, 50 m). On the other hand, the predicted *SDR_A* from the present solution is 0.76 and its relative difference is 1.3% for well at (170.76 m, 50 m). In these two cases, we demonstrate that the present solution can be used as a design tool to determine the well location for a specific amount of filtration water from nearby streams in an L-shaped aquifer.

4 Conclusions

A new semi-analytical model has been developed to analyze the 2D hydraulic head distributions with/without pumping in a heterogeneous and anisotropic aquifer for an L-shaped domain bounded by two streams with linearly varying hydraulic heads. Method of domain decomposition is used to divide the aquifer into two regions for the development of semi-analytical solution. Steady-state solution is first derived and used as the initial condition for the L-shaped aquifer system before pumping. The Laplace-domain solution of the model for transient head distribution in the aquifer subject to pumping is developed using the Fourier finite sine and cosine transform and the Laplace transform. The solution for *SDR* describing filtration rate from two streams in an L-shaped aquifer is developed based on the head solution and Darcy's law. The Stehfest algorithm is then adopted to evaluate the time-domain results for both head and *SDR* solutions in Laplace domain.

The 3D finite difference model MODFLOW is first used to support the evaluation of the hydraulic head predictions by the present solution for the L-shaped two-layered aquifer system. The hydraulic head distributions predicted by present solutions agree fairly well over the entire aquifer except the heads nearing the no-flow boundary. The solution for hydraulic head distribution in the L-shaped aquifer without pumping has been used to investigate the effect of anisotropic ratio (K_x/K_y) on

the steady-state flow system. It is interesting to note that the flow pattern in terms of lines of equal hydraulic head is strongly influenced by the value of anisotropic ratio for the region near the turning point of the L-shaped aquifer.

The transient solution for head distribution is employed to simulate the head distribution induced by pumping in the aquifer within the agriculture area of Gyeonggi-Do, Korea. The aquifer is approximated as L-shaped in this study. The simulation results indicate that the largest relative difference in predicted temporal head distributions at three piezometers by the present solution and Kihm et al.'s (2007) FEM simulation is less than 1.74%.

The *SDR* solution is first used to evaluate the steady-state *SDR* from each of the nearby streams for Yongpoong aquifer subject to a specific pumping rate. The solution is also employed to determine the temporal contribution rates from the aquifer storage and the streams toward the extraction well. Then the solution is used as a design tool to determine the well location with a specific pumping rate for required amounts of *SDR* from nearby streams. Two cases are provided with four trial pumping wells assumed at distances at least 50m from the streams. A quadratic equation is considered with the dependent variable representing the distance (d_B) from the trial well to one of the stream (stream BD) and the independent variable denoted as the estimated *SDR* (from stream AB, the main stream in Yongpoong area) predicted by the present solution at the trial pumping wells. The quadratic equation with coefficients estimated by the least squares approach is then used to determine the pumping well location for a required *SDR* from nearby streams in an L-shaped aquifer. In the case studies, the estimated *SDR* by the present solution at the well location predicted by the regression equation yields about 3.0% relative error for the required *SDR* of 0.63 and 1.3% relative error for that of 0.76. These results indicate that the present solution can be used as a preliminary design tool in determining the well location for a required amount of *SDR*.

Acknowledgements

This study was partly supported by the grants from Taiwan Ministry of Science and Technology under the contract number MOST 105-2221-E-009-043-MY2. The authors would like to thank the editor, two anonymous reviewers, and David Ferris for their valuable and constructive comments that greatly improve the manuscript.

References

Asadi-Aghbolaghi, M., and Seyyedian, H.: An analytical solution for groundwater flow to a vertical well in a triangle-shaped aquifer, Journal of Hydrology, 393, 341-348, http://dx.doi.org/10.1016/j.jhydrol.2010.08.034, 2010.

Chan, Y. K., Mullineux, N., and Reed, J. R.: Analytic solutions for drawdowns in rectangular artesian aquifers, Journal of Hydrology, 31, 151-160, http://dx.doi.org/10.1016/0022-1694(76)90026-3, 1976.

Chan, Y. K., Mullineux, N., and Reed, J. R.: Analytic solution for drawdown in an unconfined-confined rectangular aquifer, Journal of Hydrology, 34, 287-296, http://dx.doi.org/10.1016/0022-1694(77)90136-6, 1977.

Chan, Y. K., Mullineux, N., Reed, J. R., and Wells, G. G.: Analytic solutions for drawdowns in wedge-shaped artesian aquifers, Journal of Hydrology, 36, 233-246, http://dx.doi.org/10.1016/0022-1694(78)90146-4, 1978.

Charbeneau, R. J.: Groundwater Hydraulics and Pollutant Transport, Prentice Hall, Upper Saddle River, N.J, 2000.

Chen, Y.J., Yeh, H. D., and Yang, S. Y.: Analytical Solutions for Constant-Flux and Constant-Head Tests at a Finite-Diameter Well in a Wedge-Shaped Aquifer, Journal of Hydraulic Engineering, 135, 333-337, 10.1061/(ASCE)0733-9429(2009)135:4(333), 2009.

Chu, Y. J., Lin, C. C., and Yeh, H. D.: Steady-state groundwater flow in an anisotropic aquifer with irregular boundaries. International Conference on Sustainable Environmental Technologies, Bangkok, Thailand. 2012

Corapcioglu, M. Y., Borekci, O., and Haridas, A.: Analytical solutions for rectangular aquifers with third-kind (Cauchy) boundary conditions, Water Resources Research, 19, 523-528, 10.1029/WR019i002p00523, 1983.

Daly, C. J., and Morel-Seytoux, H. J.: An integral transform method for the linearized Boussinesq Groundwater Flow Equation, Water Resources Research, 17, 875-884, 10.1029/WR017i004p00875, 1981.

Driscoll, F.G.: Groundwater and Wells, 2nd ed. Johnson Screens, Minnesota. 1986.

Falade, G. K.: On the flow of fluid in the wedged anisotropic porous domain, Journal of Hydrology, 58, 111-121, http://dx.doi.org/10.1016/0022-1694(82)90072-5, 1982.

Holzbecher, E.: Analytical solution for two-dimensional groundwater flow in presence of two isopotential lines, Water Resources Research, 41, n/a-n/a, 10.1029/2005WR004583, 2005.

Huang, C. S., Chen, J. J., and Yeh, H. D.: Approximate analysis of three-dimensional groundwater flow toward a radial collector well in a finite-extent unconfined aquifer, Hydrol. Earth Syst. Sci., 20, 55-71, 10.5194/hess-20-55-2016, 2016.

Jafari, F., Javadi, S., Golmohammadi, G., Karimi, N., and Mohammadi, K.: Numerical simulation of groundwater flow and aquifer-system compaction using simulation and InSAR technique: Saveh basin, Iran, Environmental Earth Sciences, 75, 833, 10.1007/s12665-016-5654-x, 2016.

Kantorovich, L.V., Krylov, V. I.: Approximate Methods of Higher Analysis. Interscience, New York, 1958.

Kacimov, A. R., Kayumov, I. R., Al-Maktoumi, A.: Rainfall induced groundwater mound in wedge-shaped promontories: The Strack–Chernyshov model revisited. Advances in Water Resources, 97, 110–119, http://dx.doi.org/10.1016/j.advwatres.2016.08.011, 2016.

Kacimov, A. R., Maklakov, D. V., Kayumov, I. R., Al-Futaisi, A.: Free Surface flow in a microfluidic corner and in an unconfined aquifer with accretion: The Signorini and Saint-Venant analytical techniques revisited. Transport in Porous Media, 116(1), DOI 10.1007/s11242-016-0767-y, 115–142, 2017.

Kihm, J.-H., Kim, J.-M., Song, S.-H., and Lee, G.-S.: Three-dimensional numerical simulation of fully coupled groundwater flow and land deformation due to groundwater pumping in an unsaturated fluvial aquifer system, Journal of Hydrology, 335, 1-14, http://dx.doi.org/10.1016/j.jhydrol.2006.09.031, 2007.

Kuo, M. C. T., Wang, W. L., Lin, D. S., Lin, C. C., and Chiang, C. J.: An Image-Well Method for Predicting Drawdown Distribution in Aquifers with Irregularly Shaped Boundaries, Ground Water, 32, 794-804, 10.1111/j.1745-6584.1994.tb00921.x, 1994.

Lambs, L.: Interactions between groundwater and surface water at river banks and the confluence of rivers, Journal of
5   Hydrology, 288, 312-326, http://dx.doi.org/10.1016/j.jhydrol.2003.10.013, 2004.

Latinopoulos, P.: Well recharge in idealized rectangular aquifers, Advances in Water Resources, 5, 233-235, http://dx.doi.org/10.1016/0309-1708(82)90006-9, 1982.

Latinopoulos, P.: Periodic recharge to finite aquifers from rectangular areas, Advances in Water Resources, 7, 137-140, http://dx.doi.org/10.1016/0309-1708(84)90043-5, 1984.

10   Latinopoulos, P.: Analytical solutions for periodic well recharge in rectangular aquifers with third-kind boundary conditions, Journal of Hydrology, 77, 293-306, http://dx.doi.org/10.1016/0022-1694(85)90213-6, 1985.

Li, P., Stagnitti, F., and Das, U.: A new analytical solution for Laplacian porous-media flow with arbitrary boundary shapes and conditions, Mathematical and Computer Modelling, 24, 3-19, http://dx.doi.org/10.1016/S0895-7177(96)00160-4, 1996.

Li, H., and Jiao, J. J.: Tidal groundwater level fluctuations in L-shaped leaky coastal aquifer system, Journal of Hydrology,
15   268, 234-243, http://dx.doi.org/10.1016/S0022-1694(02)00177-4, 2002.

Loudyi, D., Falconer, R. A., and Lin, B.: Mathematical development and verification of a non-orthogonal finite volume model for groundwater flow applications, Advances in Water Resources, 30, 29-42, 10.1016/j.advwatres.2006.02.010, 2007.

Lu, C., Xin, P., Li, L., and Luo, J.: Steady state analytical solutions for pumping in a fully bounded rectangular aquifer, Water Resources Research, 51, 8294-8302, 10.1002/2015WR017019, 2015.

20   Matthews, C. S., Brons, F., and Hazebroek, P.: A method for determination of average pressure in bounded reservoir, Trans. AIME, 201, 182-191, 1954.

Mackowski, D. W.: Conduction Heat Transfer: Notes for MECH 7210. Mechanical Engineering Department, Auburn University, 2011.

Mahdavi, A., Seyyedian, H.: Steady-state groundwater recharge in trapezoidal-shaped aquifers: A semi-analytical approach
25   based on variational calculus. Journal of Hydrology, 512, 457–462, https://doi.org/10.1016/j.jhydrol.2014.03.014, 2014.

Mohanty, S., Jha, M. K., Kumar, A., and Panda, D. K.: Comparative evaluation of numerical model and artificial neural network for simulating groundwater flow in Kathajodi–Surua Inter-basin of Odisha, India, Journal of Hydrology, 495, 38-51, http://dx.doi.org/10.1016/j.jhydrol.2013.04.041, 2013.

Patel, A., and Serrano, S. E.: Decomposition solution of multidimensional groundwater equations, Journal of Hydrology, 397,
30   202-209, http://dx.doi.org/10.1016/j.jhydrol.2010.11.032, 2011.

Read, W. W., and Volker, R. E.: Series solutions for steady seepage through hillsides with arbitrary flow boundaries, Water Resources Research, 29, 2871-2880, 10.1029/93WR00905, 1993.

Rhms 2013, available at: http://mobile.river.go.kr/Mobiles/sub_03/Books/%ED%95%9C%EA%B5%AD%ED%95%98%EC%B2%9C%EC%9D%BC%EB%9E%8C(2012.12.31%EA%B8%B0%EC%A4%80).pdf, last accessed on 04 September 2017. (in Korean)

Samani, N., and Zarei-Doudeji, S.: Capture zone of a multi-well system in confined and unconfined wedge-shaped aquifers, Advances in Water Resources, 39, 71-84, http://dx.doi.org/10.1016/j.advwatres.2012.01.004, 2012.

Samani, N., and Sedghi, M. M.: Semi-analytical solutions of groundwater flow in multi-zone (patchy) wedge-shaped aquifers, Advances in Water Resources, 77, 1-16, http://dx.doi.org/10.1016/j.advwatres.2015.01.003, 2015.

Serrano, S. E.: A simple approach to groundwater modelling with decomposition, Hydrological Sciences Journal, 58, 177-185, 10.1080/02626667.2012.745938, 2013.

Stehfest, H.: Algorithm 368: Numerical inversion of Laplace transforms, Commun. ACM, 13, 47-49, 10.1145/361953.361969, 1970.

Sun, H.: A two-dimensional analytical solution of groundwater response to tidal loading in an estuary, Water Resources Research, 33, 1429-1435, 10.1029/97WR00482, 1997.

Taigbenu, A. E.: Green element simulations of multiaquifer flows with a time-dependent Green's function, Journal of Hydrology, 284, 131-150, http://dx.doi.org/10.1016/j.jhydrol.2003.07.002, 2003.

Todd, D. K., and Mays, L. W.: Groundwater Hydrology, 3rd ed, Wiley, 2005.

U.S. Geological Survey: MODFLOW-2005: The U.S. geological survey modular groundwater model- the groundwater flow process. U.S. Geological Survey Techniques and Methods 6-A16, 2005

Yeh, H.-D., Chang, Y.-C., and Zlotnik, V. A.: Stream depletion rate and volume from groundwater pumping in wedge-shape aquifers, Journal of Hydrology, 349, 501-511, http://dx.doi.org/10.1016/j.jhydrol.2007.11.025, 2008.

Appendix A. Steady-state solution for flow in an L-shaped aquifer without pumping

On the basis of dimensionless variables and parameters defined in Sect. 2.2, Eqs. (1) and (2) can be written respectively as

$$\kappa_1 \frac{b_2^2}{l_1^2} \frac{\partial^2 \phi_1^*}{\partial x^{*2}} + \frac{\partial^2 \phi_1^*}{\partial y^{*2}} = \frac{\partial \phi_1^*}{\partial t^*} - \sum_{k=1}^{M} Q_{1k}^* \delta(x^* - x_{1k}^*) \delta(y^* - y_{1k}^*)$$

$$0 \le x^* \le l_1^*, 0 \le y^* \le d_1^* \tag{A1}$$

and

$$\kappa_2 \frac{d_2^2}{l_1^2} \frac{\partial^2 \phi_2^*}{\partial x^{*2}} + \frac{\partial^2 \phi_2^*}{\partial y^{*2}} = \frac{S_{s2}}{S_{s1}} \frac{K_{y1}}{K_{y2}} \frac{\partial \phi_2^*}{\partial t^*} - \sum_{l=1}^{N} Q_{2l}^* \delta(x^* - x_{2l}^*) \delta(y^* - y_{2l}^*)$$

$$0 \le x^* \le l_2^*, d_1^* \le y^* \le 1 \tag{A2}$$

The dimensionless boundary conditions for region 1 can be expressed as:

$$\phi_1^*(0, y^*) = 0 \text{ for boundary AG} \tag{A3}$$

$$\phi_1^*(1, y^*) = h_{31}^* + h_{23}^* y^* \text{ for boundary BC} \tag{A4}$$

$$\phi_1^*(x^*, 0) = h_{31}^* x^* \text{ for boundary AB} \tag{A5}$$

$$\frac{\partial \phi_1^*}{\partial y^*}(x^*, d_1^*) = 0 \text{ for GF} \tag{A6}$$

and for region 2 are

$$\frac{\partial \phi_2^*}{\partial x^*}(l_2^*, y^*) = 0 \text{ for boundary EF} \tag{A7}$$

$$\phi_2^*(1, y^*) = h_{31}^* + h_{23}^* y^* \text{ for boundary CD} \tag{A8}$$

$$\phi_2^*(x^*, 1) = h_{21}^* \text{ for boundary DE} \tag{A9}$$

The continuity requirements of hydraulic head and flux at the region interface in dimensionless form are respectively expressed as

$$h_1 \phi_1^*(x^*, d_1^*) = h_2 \phi_2^*(x^*, d_1^*) \text{ for segment CF} \tag{A10}$$

and

$$K_{y1} h_1 \frac{\partial \phi_1^*}{\partial y^*}\Big|_{y^* = d_1^*} = K_{y2} h_2 \frac{\partial \phi_2^*}{\partial y^*}\Big|_{y^* = d_1^*} \text{ for segment CF} \tag{A11}$$

The steady-state solution for groundwater flow in an L-shaped aquifer without pumping can be solved after removing the source/sink term in Eqs. (A1) and (A2). Multiplying Eq. (A1) by $sin(\lambda_m x^*)$ and integrating it for x^* from 0 to 1 in region 1 with boundary conditions Eqs. (A3) and (A4), Eq. (A1) is then transformed to

$$\Omega_{1m}^2 \bar{\phi}_1^* - \frac{\partial^2 \bar{\phi}_1^*}{\partial y^{*2}} = -\kappa_1 \frac{d_2^2}{l_1^2} \lambda_m (-1)^m (h_{31}^* + h_{23}^* y^*) \tag{A12}$$

with

$$\bar{\phi}_1^* = \int_0^1 \phi_1^* sin(\lambda_m x^*) dx^* \tag{A13}$$

where $\Omega_{1m} = \lambda_m \sqrt{\kappa_1} \, d_2 / l_1$, $\lambda_m = m\pi$ and $m = 1, 2, 3, \dots$.

Similarly, Eq. (A2) can be transformed via multiplying Eq. (A2) by $cos[\alpha_n(x^* - l_2^*)]$ and integrating it for x^* from l_2^* to 1 in region 2 with boundary conditions Eqs. (A7) and (A8). The result is

$$\Omega_{2n}^2 \bar{\phi}_2^* - \frac{\partial^2 \bar{\phi}_2^*}{\partial y^{*2}} = \kappa_2 \frac{d_2^2}{l_1^2} \alpha_n (-1)^{n-1} (H_{31}^* + H_{23}^* y^*) \tag{A14}$$

with

$$\bar{\phi}_2^* = \int_{l_2^*}^1 \phi_2^* \cos[\alpha_n(x^* - l_2^*)]dx^* \tag{A15}$$

where $\Omega_{2n} = \alpha_n\sqrt{\kappa_2}\, d_2/l_1$, $\alpha_n = (n - 1/2)\pi/(1 - l_2^*)$ and $n = 1,2,3, ...$

The general solutions of Eqs. (A12) and (A14) can be written respectively as

$$\bar{\phi}_1^*(m, y^*) = C_{1m}e^{\Omega_{1m}y^*} + C_{2m}e^{-\Omega_{1m}y^*} - \frac{(-1)^m}{\lambda_m}(h_{31}^* + h_{23}^* y^*) \tag{A16}$$

5 and

$$\bar{\phi}_2^*(n, y^*) = D_{1n}e^{\Omega_{2n}y^*} + D_{2n}e^{-\Omega_{2n}y^*} - \frac{(-1)^{n-1}}{\alpha_n}(H_{31}^* + H_{23}^* y^*) \tag{A17}$$

The coefficients C_{1m} and C_{2m} in Eq. (A16) are determined by Eq. (A5) and the result is

$$C_{2m} = -C_{1m} \tag{A18}$$

Similarly, the coefficients D_{1n} and D_{2n} in Eq. (A17) are determined based on Eq. (A10) as

10 $$D_{1n} = -D_{2n}e^{-2\Omega_{2n}} \tag{A19}$$

Substituting Eq. (A18) into Eq. (A16), the inversion of $\bar{\phi}_1^*$ leads to Eq. (12) for dimensionless hydraulic head distribution in region 1. Similarly, the inversion of $\bar{\phi}_2^*$ for region 2 after substituting Eq. (A19) into Eq. (A17) results in Eq. (13).   Based on Eqs. (A10) and (A11), the coefficients of C_{1m} and D_{2n} can be simultaneously determined and the results are respectively given in Eqs. (18) and (19).

15 **Appendix B. Transient solutions for an L-shaped aquifer**

Multiplying Eq. (A1) by $\sin(\lambda_i x^*)$ and integrating it for x^* from 0 to 1 in region 1 with Eqs. (A3) and (A4), Eq. (A1) can be transformed as

$$-\Omega_{1i}^2\bar{\phi}_1^* - \theta_1^2\lambda_i(-1)^i(h_{31}^* + h_{23}^* y^*) + \frac{\partial^2\bar{\phi}_1^*}{\partial y^{*2}} = \frac{\partial\bar{\phi}_1^*}{\partial t^*} - \sum_{k=1}^M Q_{1k}^* \sin(\lambda_i x_{1k}^*)\,\delta(y^* - y_{1k}^*) \tag{B1}$$

with

20 $$\bar{\phi}_1^* = \int_0^1 \phi_1^* \sin(\lambda_i x_{1k}^*)\,dx^* \tag{B2}$$

where $\Omega_{1i} = \lambda_i\sqrt{\kappa_1}\, d_2/l_1$, $\theta_1 = \sqrt{\kappa_1}d_2/l_1$, and $\lambda_i = i\pi$, $i = 1,2,3, ...$

Similarly, Eq. (A2) can be transformed via multiplying Eq. (A2) by $\cos(\alpha_j x^*)$ and integrating it for x^* from l_2^* to 1 in region 2 with Eqs. (A7) and (A8). The result is

$$-\Omega_{2j}^2\bar{\phi}_2^* + \theta_2^2\alpha_j(-1)^j(H_{31}^* + H_{23}^* y^*) + \frac{\partial^2\bar{\phi}_2^*}{\partial y^{*2}} = \frac{K_{y1}S_{s2}}{K_{y2}S_{s1}}\frac{\partial\bar{\phi}_2^*}{\partial t^*} - \sum_{l=1}^N Q_{2l}^* \cos(\alpha_j x_{2l}^*)\,\delta(y^* - y_{2l}^*) \tag{B3}$$

with

$$\bar{\phi}_2^* = \int_{l_2^*}^1 \phi_2^* \cos(\alpha_j x_{2l}^*) \, dx^* \tag{B4}$$

where $\Omega_{2j} = \alpha_j \sqrt{\kappa_2} d_2/l_1$, $\theta_2 = \sqrt{\kappa_2} d_2/l_1$, and $\alpha_j = (1 - 1/2)\pi/(1 - l_2^*)$ for $j = 1,2,3, \dots$

Then, taking Laplace transforms to Eq. (B1) results in

$$-\Omega_{1i}^2 \bar{\bar{\phi}}_1^* - \frac{1}{p}\theta_1^2 \lambda_i (-1)^i (h_{31}^* + h_{23}^* y^*) + \frac{\partial^2 \bar{\bar{\phi}}_1^*}{\partial y^{*2}} = p\bar{\bar{\phi}}_1^* - \bar{\phi}_{1s}^* - \frac{1}{p}\sum_{k=1}^M Q_{1k}^* \sin(\lambda_i x_{1k}^*) \delta(y^* - y_{1k}^*) \tag{B5}$$

where $\bar{\phi}_{1s}^*$ is the steady state solution of region 1. Hence, Eq. (B5) can be organized as:

$$-\mu_i^2 + \bar{\bar{\phi}}_1^* + \frac{\partial^2 \bar{\bar{\phi}}_1^*}{\partial y^{*2}} = \frac{1}{p}\theta_1^2 \lambda_i (-1)^i (h_{31}^* + h_{23}^* y^*) - \sum_{m=1}^\infty \Delta_1 [C_{1m} E_1(m, y^*) + F_1(m, y^*)] \left(\frac{1}{2} - \frac{\sin 2\lambda_i}{4\lambda_i}\right) -$$

$$\frac{1}{p}\sum_{k=1}^M Q_{1k}^* \sin(\lambda_i x_{1k}^*) \delta(y^* - y_{1k}^*) \tag{B6}$$

where $\mu_i = \sqrt{\theta_1^2 \lambda_i^2 + p}$ with the Laplace transform of $\bar{\phi}_1^*$ defined as:

$$\bar{\bar{\phi}}_1^*(i, y^*, p) = \int_0^\infty \bar{\phi}_1^*(i, y^*, t) e^{-pt^*} dt^* \tag{B7}$$

Similarly, the Laplace transform of Eq. (B3) is obtained as:

$$-\Omega_{2j}^2 \bar{\phi}_2^* + \frac{1}{p}\theta_2^2 \alpha_j (-1)^j (H_{31}^* + H_{23}^* y^*) + \frac{\partial^2 \bar{\phi}_2^*}{\partial y^{*2}} = \frac{K_{y1} S_{s2}}{K_{y2} S_{s1}}(p\bar{\bar{\phi}}_2^* - \bar{\phi}_{2s}^*) - \frac{1}{p}\sum_{l=1}^N Q_{2l}^* \cos(\alpha_j x_{2l}^*) \delta(y^* - y_{2l}^*) \tag{B8}$$

where $\bar{\phi}_{2s}^*$ is the steady state solution of region 2. Thus, Eq. (B8) can be written as:

$$-\theta_j^2 \bar{\bar{\phi}}_2^* + \frac{\partial^2 \bar{\bar{\phi}}_2^*}{\partial y^{*2}} = -\frac{1}{p}\theta_2^2 \alpha_j (-1)^j (H_{31}^* + H_{23}^* y^*) - \frac{K_{y1} S_{s2}}{K_{y2} S_{s1}}\sum_{n=1}^\infty \Delta_2 [D_{2n} E_2(m, y^*) + F_2(m, y^*)] \cos[\alpha_j(x^* - l_2^*)] -$$

$$\frac{1}{p}\sum_{l=1}^N Q_{2l}^* \cos(\alpha_j x_{2l}^*) \delta(y^* - y_{2l}^*) \tag{B9}$$

where $\theta_j = \sqrt{\theta_2^2 \alpha_j^2 + p s_{s2} k_{y1}/s_{s1} k_{y2}}$ with the Laplace transform of $\bar{\phi}_2^*$ defined as:

$$\bar{\bar{\phi}}_2^*(j, y^*, p) = \int_0^\infty \bar{\phi}_2^*(j, y^*, t) e^{-pt^*} dt^* \tag{B10}$$

The general solution of Eq. (B6) can be expressed as:

$$\bar{\bar{\phi}}_1^*(i, y^*, p) = T_{1i} e^{\mu_i y^*} + T_{2i} e^{-\mu_i y^*} + \bar{\bar{\phi}}_{1p}^*(i, y^*, p) \tag{B11}$$

where the particular solution $\bar{\bar{\phi}}_{1p}^*(i, y^*, p)$ is

$$\bar{\bar{\phi}}_{1p}^*(i, y^*, p) = \frac{e^{\mu_i y^*}}{2\mu_i} \int e^{-\mu_i y^*} \Delta_{1y}(i, y^*, p) dy^* - \frac{e^{-\mu_i y^*}}{2\mu_i} \int e^{\mu_i y^*} \Delta_{1y}(i, y^*, p) dy^* \tag{B12}$$

with

$$\Delta_{1y}(i, y^*, p) = \frac{1}{p}\theta_1^2\lambda_i(-1)^i(h_{31}^* + h_{23}^* y^*) - \sum_{m=1}^{\infty}\Delta_1[C_{1m}E_1(m, y^*) + F_1(m, y^*)]\left(\frac{1}{2} - \frac{sin2\lambda_i}{4\lambda_i}\right) -$$

$$\frac{1}{p}\sum_{k=1}^{M} Q_{1k}^* sin(\lambda_i x_{1k}^*)\,\delta(y^* - y_{1k}^*)$$ (B13)

Moreover, Eq. (B9) can also be expressed as:

$$\bar{\bar{\phi}}_2^*(j, y^*, p) = T_{1j}e^{\theta_j y^*} + T_{2j}e^{-\theta_j y^*} + \bar{\bar{\phi}}_{2p}^*(j, y^*, p)$$ (B14)

in which $\bar{\bar{\phi}}_{2p}^*(j, y^*, p)$ is

$$\bar{\bar{\phi}}_{2p}^*(j, y^*, p) = \frac{e^{\theta_j y^*}}{2\theta_j}\int e^{-\theta_j y^*}\Delta_{2y}(j, y^*, p)dy^* - \frac{e^{-\theta_j y^*}}{2\theta_j}\int e^{\theta_j y^*}\Delta_{2y}(i, y^*, p)dy^*$$ (B15)

with

$$\Delta_{2y}(j, y^*, p) = -\frac{1}{p}\theta_2^2\alpha_j(-1)^j(H_{31}^* + H_{23}^* y^*) - \frac{K_{y1}S_{s2}}{K_{y2}S_{s1}}\sum_{n=1}^{\infty}\Delta_2[D_{2n}E_2(m, y^*) + F_2(m, y^*)]cos[\alpha_j(x^* - l_2^*)] -$$

$$\frac{1}{p}\sum_{l=1}^{N}Q_{2l}^* cos(\alpha_j x_{2l}^*)\,\delta(y^* - y_{2l}^*)$$ (B16)

On the basis of Eq. (A5), the coefficient T_{2i} in Eq. (B11) can be determined in terms of T_{1i} as:

$$T_{2i} = -h_{31}^*\frac{(-1)^i}{\lambda_i} + \frac{h_{31}^*}{p\mu_i^2}[\theta_1^2\lambda_i(-1)^i] + \Delta_1(-1)^i C_{1m}\left(\frac{1}{2} - \frac{sin2\lambda_i}{4\lambda_i}\right) - T_{1i}$$ (B17)

The solution for hydraulic head distribution in region 1 is given as Eq. (26) which is obtained by substituting Eq. (B17) into Eq. (B11) and then taking the following inverse Fourier transform to Eq. (B11) denoted as:

$$\tilde{\phi}_1^*(x^*, y^*, p) = \sum_{i=0}^{\infty}\bar{\bar{\phi}}_1^*(i, y^*, p)sin(\lambda_i x^*)$$ (B18)

with

$$w_{1i}^* = T_{1i}(e^{\mu_i y^*} - 1)\big|_{y^*=d_1^*} - \frac{1}{2\mu_i p}\sum_{k=1}^{M}Q_{1k}^* sin(\lambda_i x_{1k}^*)[e^{\mu_i(y^* - y_{1k}^*)} - e^{\mu_i(y_{1k}^* - y^*)}]\big|_{y^*=d_1^*}$$ (B19)

Similarly, T_{1j} in Eq. (B14) can be obtained based on Eq. (A9) as:

$$T_{1j} = T_{2j}e^{-2\theta_j} - \left[\frac{\theta_2^2\alpha_j(-1)^j}{p} + \frac{K_{y1}S_{s2}(-1)^j}{K_{y2}S_{s1}\alpha_j}\right]\frac{H_{21}^* e^{-\theta_j}}{\theta_j^2} + \frac{H_{21}^* e^{-\theta_j}(-1)^j}{\alpha_j p} + \frac{1}{p}\sum_{l=1}^{N}Q_{2l}^* cos(\alpha_j x_{2l}^*)\frac{e^{-\theta_j y_{2l}^*} - e^{\theta_j(y_{2l}^*-2)}}{2\theta_j}$$ (B20)

The solution for region 2 is Eq. (27) which is acquired by substituting Eq. (B20) into Eq. (B14) then taking the following inverse Fourier transform to Eq. (B14) expressed as:

$$\tilde{\phi}_2^*(x^*, y^*, p) = \sum_{j=0}^{\infty}\bar{\bar{\phi}}_2^*(j, y^*, p)cos(\alpha_j x^*)$$ (B21)

with

$$w_{2j}^* = T_{2j} \tag{B22}$$

Furthermore, the coefficients of w_{1i}^* and w_{2j}^* can be simultaneously determined by Eqs. (A10) and (A11). The results are respectively given in Eqs. (36) and (37).

Table 1 Notations used in the text.

Notation	Definition
ϕ_1, ϕ_2	Hydraulic head for region 1 and 2. [L]
Q_{1k}, Q_{2k}	Unit thickness pumping rate for region 1 and 2. [L^2/T]
S_{s1}, S_{s2}	Specific storage for region 1 and 2. [L^{-1}]
K_x, K_y	Hydraulic conductivities in x- and y-direction. [L/T]
t	Time. [T]
p	Laplace variable.
h_1, h_2, h_3	Hydraulic heads at boundaries AG, DE and point B, respectively. [L]
l_1, l_2	Length of boundary FG and AB. [L]
d_1, d_2	Length of boundary BC and CD. [L]
κ_1, κ_2	Anisotropic ratio of hydraulic conductivity in region 1 and 2.
Δ_1	$\begin{cases} 1, & m = 0 \\ 2, & m \neq 0 \end{cases}, m = 1,2,3, \dots$
Δ_2	$\frac{2}{1-l_2^*}$.
λ_v	$\frac{v\pi}{l_1^*}, v = m, i = 1,2,3, \dots$
α_w	$\frac{(w-1/2)\pi}{1-l_2^*}, w = n, j = 1,2,3, \dots$
Ω_{1v}	$\lambda_v \sqrt{\kappa_1}\, d_2/l_1 , v = m, i = 1,2,3, \dots$
Ω_{2w}	$\alpha_w \sqrt{\kappa_2}\, d_2/l_1 , w = n, j = 1,2,3, \dots$
h_{21}^{*}	$(h_2 - h_1)/h_1$
h_{23}^{*}	$(h_2 - h_3)/h_1$
h_{31}^{*}	$(h_3 - h_1)/h_1$
H_{21}^{*}	$(h_2 - h_1)/h_2$
H_{23}^{*}	$(h_2 - h_3)/h_2$
H_{31}^{*}	$(h_3 - h_1)/h_2$

δ_1	2
δ_2	$\dfrac{2}{1 - l_2^*}$
θ_1	$\sqrt{\kappa_1(d_2^2/l_1^2)}$
θ_2	$\sqrt{\kappa_2(d_2^2/l_1^2)}$
μ_i	$\sqrt{\theta_1^2 \lambda_i^2 + p},\ i = 1,2,3,\dots$
θ_j	$\sqrt{\theta_2^2 \alpha_j^2 + p s_{s2} k_{y1}/s_{s1} k_{y2}},\ j = 1,2,3,\dots$

Figures

Figure 1: Location of the fluvial aquifer. Note that this figure is modified from Google Earth.
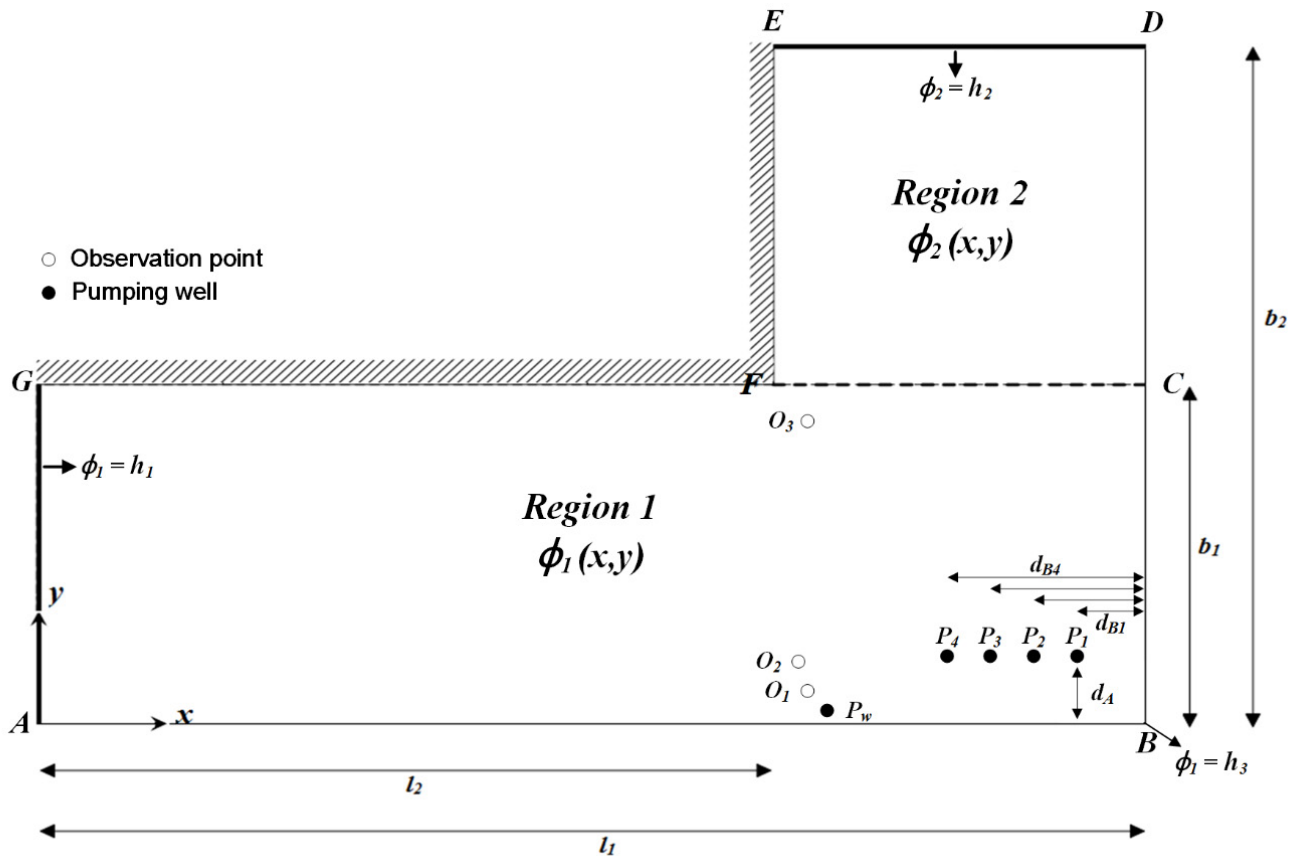
Figure 2: The L-Shaped fluvial aquifer with two sub-regions.
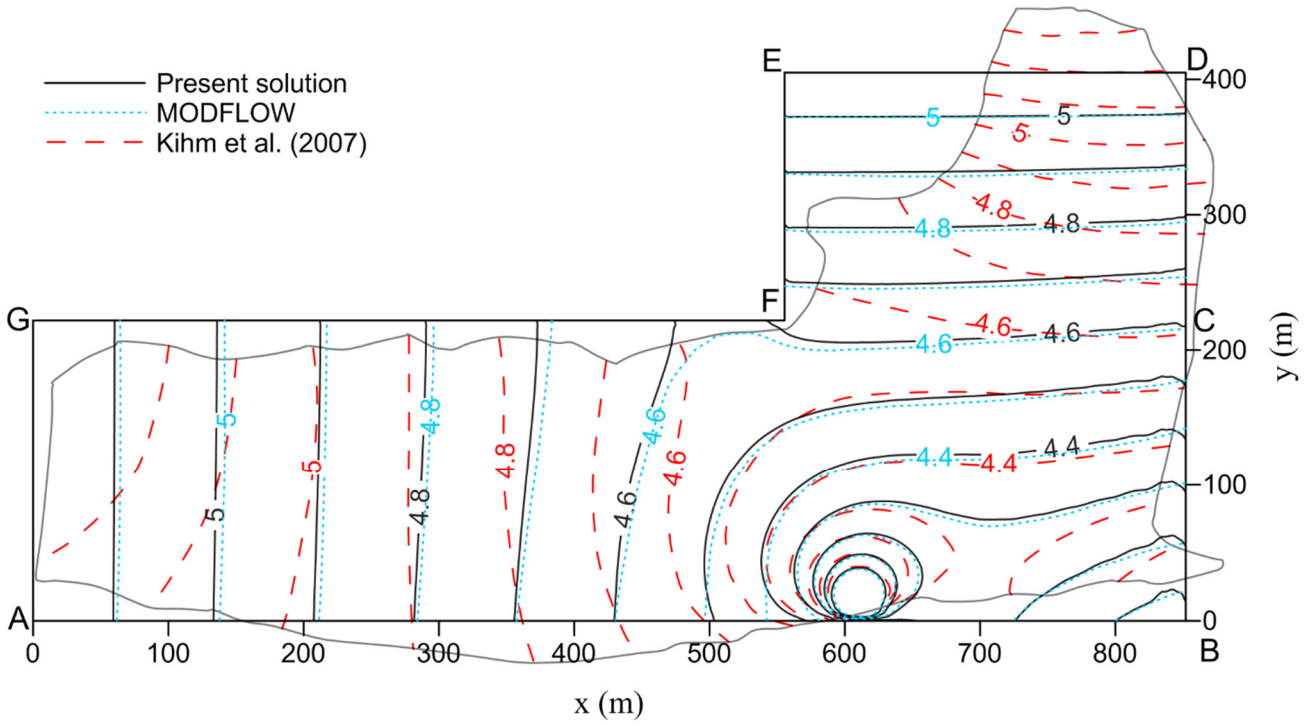
Figure 3: Contours of hydraulic head in L-shaped aquifer predicted by the present solution, MODFLOW, and FEM simulations with irregular outer boundary reported in Kihm et al. (2007).
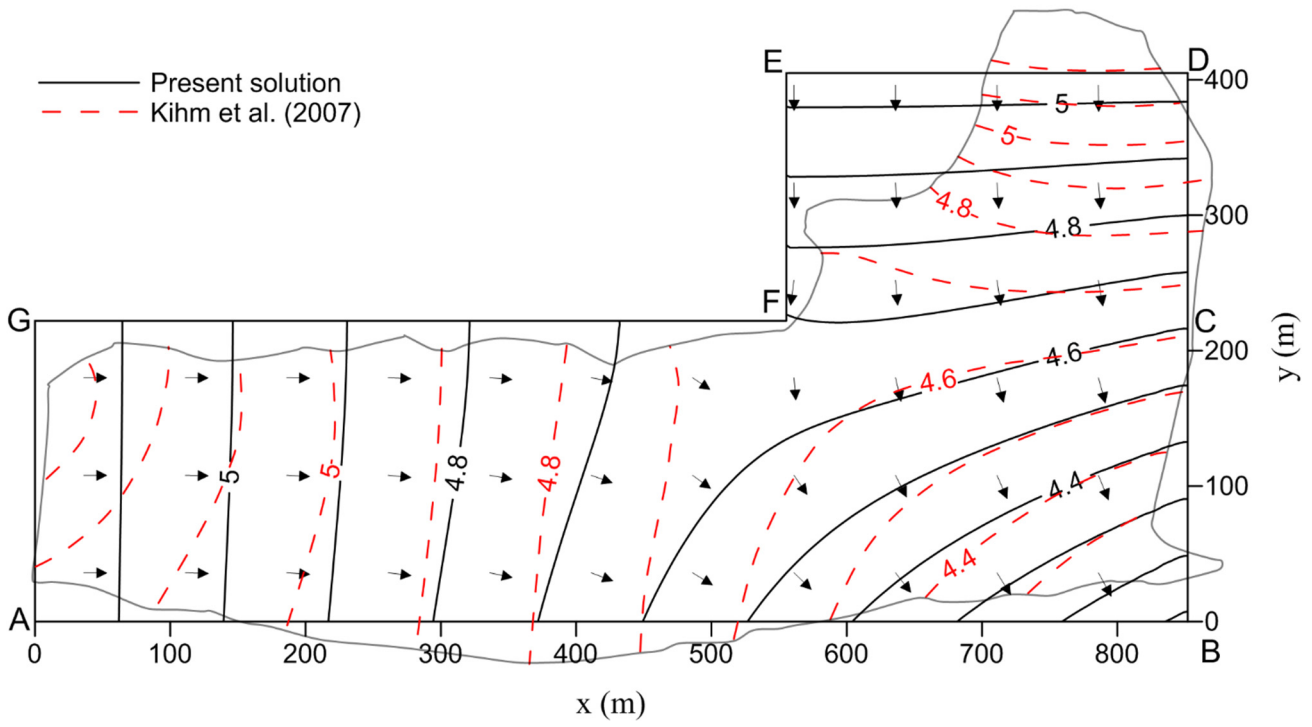
Figure 4: Steady-state hydraulic head contours without pumping in Yongpoong 2 Agriculture District.
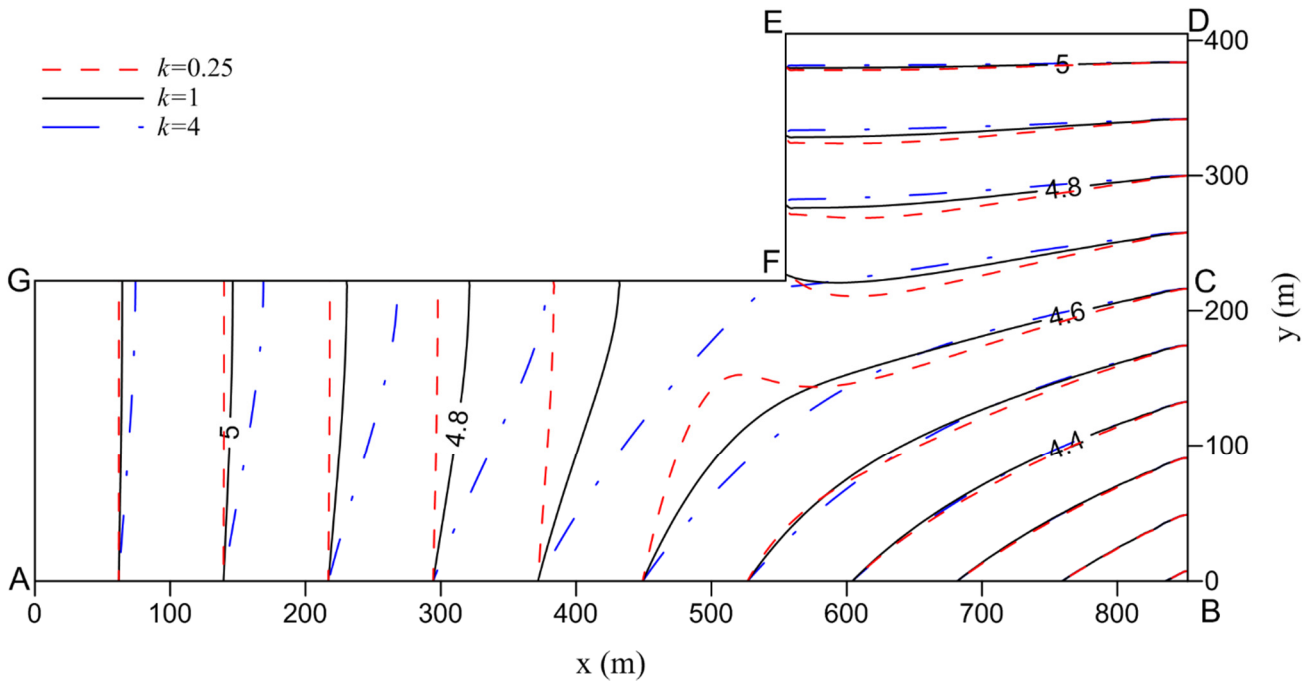
Figure 5: Steady-state hydraulic head contours in the L-shaped aquifers with three different anisotropy ratios for $\kappa_1 = \kappa_2 = \kappa$.
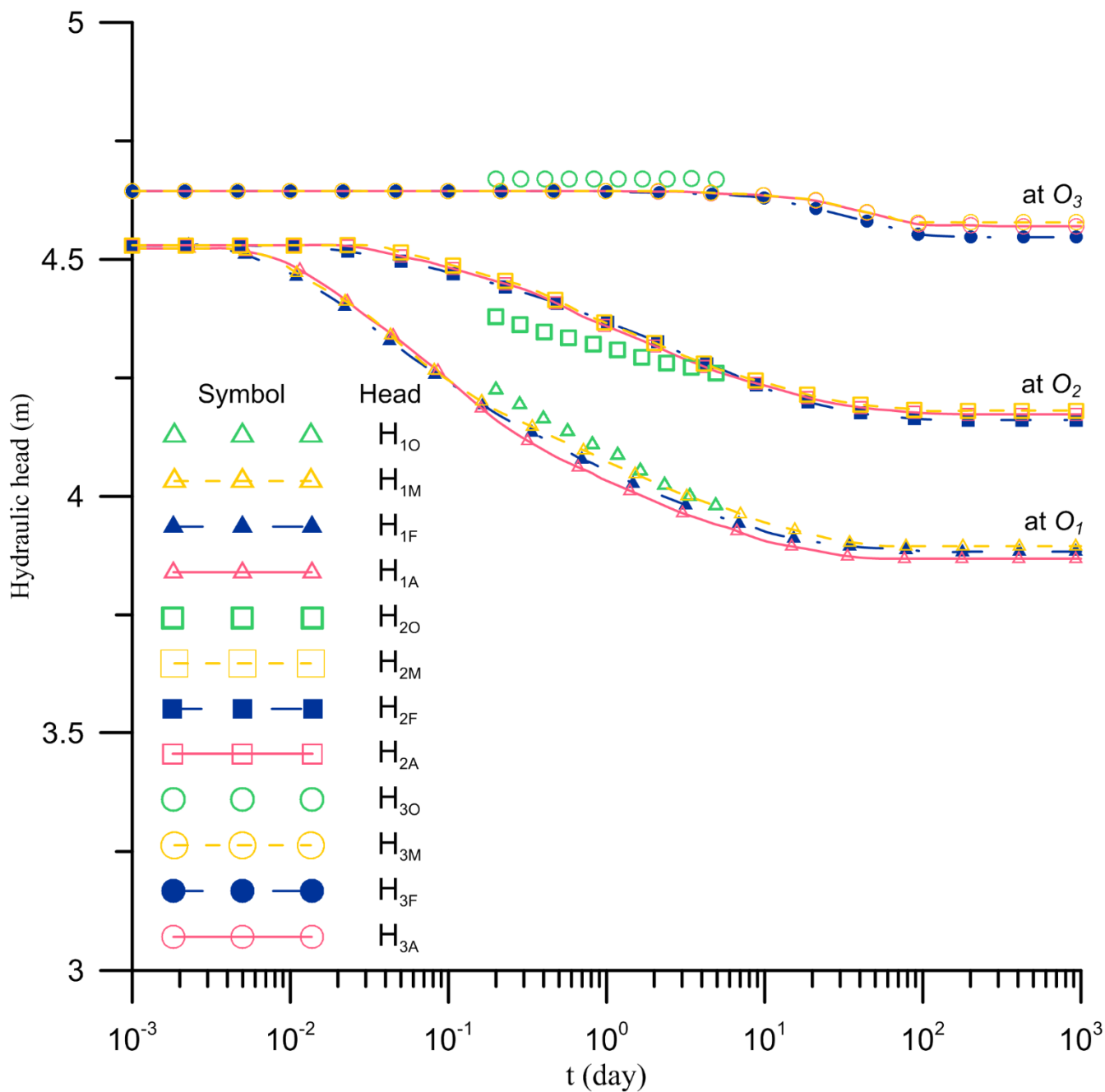
Figure 6: Temporal distributions of hydraulic head H_{io} **observed at piezometer** O_i **and** H_{iF} **simulated by the FEM simulations both reported in Kihm et al. (2007) and** H_{iA} **and** H_{iM} **predicted by the present solution and MODFLOW, respectively, for** $i = 1, 2, 3$.
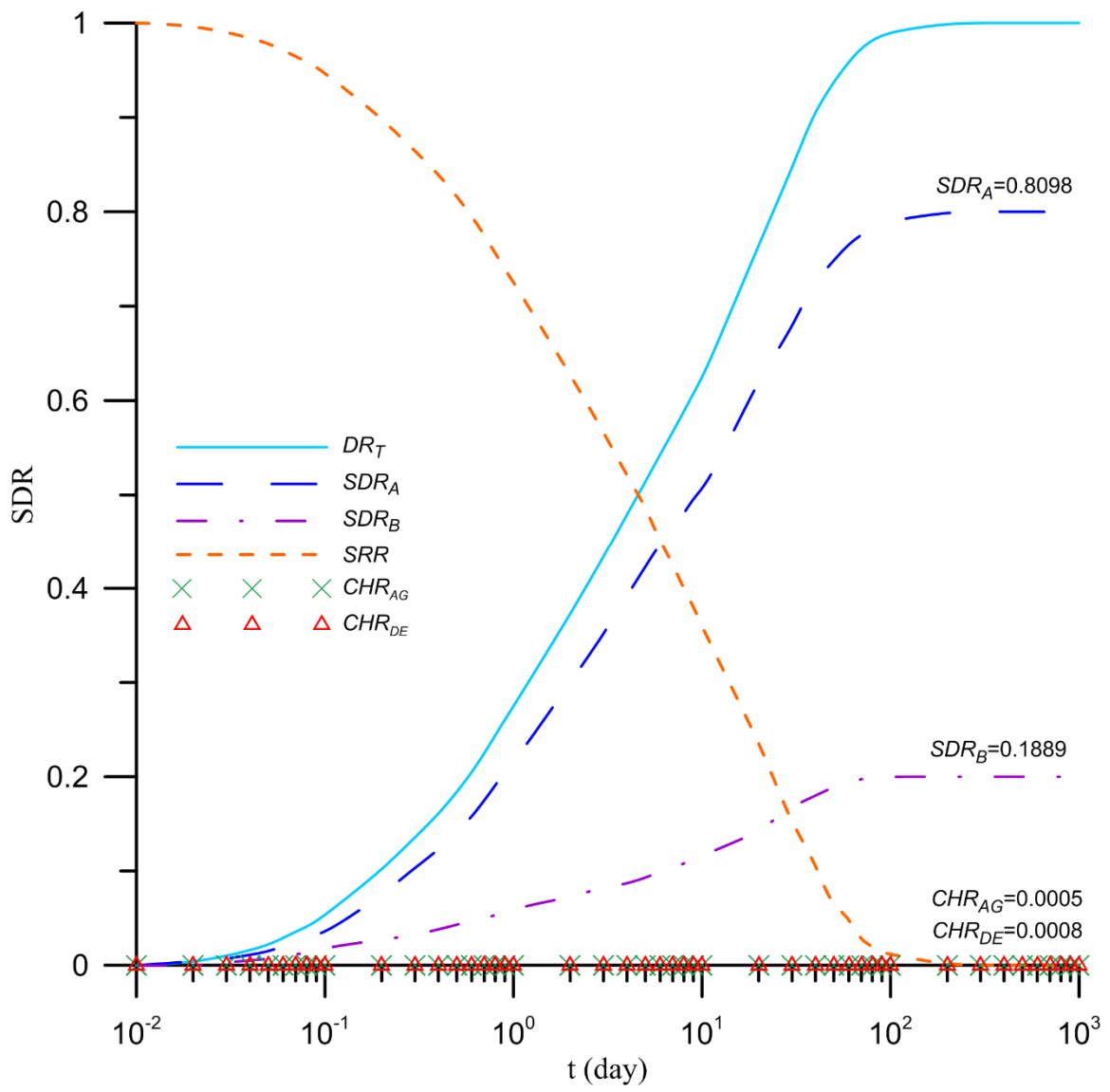
Figure 7: Temporal distributions of *SDRs*, *CHRs* and *SRR* due to pumping at P_w